Flow split characterization of two immiscible phases with different wettability scenarios: A numerical investigation using a coupled Cahn-Hilliard and Navier-Stokes system

Kai Bao, Amgad Salama, Shuyu Sun

Citation:
Kai Bao, Amgad Salama, Shuyu Sun(2018). Flow split characterization of two immiscible phases with different wettability scenarios: A numerical investigation using a coupled Cahn-Hilliard and Navier-Stokes system. International Journal of Multiphase Flow, 2018, 100, 172-185 DOI: 10.1016/j.ijmultiphaseflow.2017.12.016

Flow split characterization of two immiscible phases with different wettability scenarios: a numerical investigation using a coupled Cahn-Hilliard and Navier-Stokes system

Kai Bao[1], Amgad Salama[2,*], and Shuyu Sun[3]

[1]SINTEF, Department of Applied Mathematics, Forskningsveien 1, 0373, Oslo, Norway

[2]Faculty of Engineering, University of Regina, Regina, Sk., Canada

[3]King Abdullah University of Science and Technology (KAUST), Thuwal 23955-6900, KSA

(*email: amgad.salama@uregina.ca)

Abstract

Numerical investigation of flow branching of two-phase immiscible fluids in a Y-shaped, planner channel is conducted by solving the coupled Cahn-Hilliard and Naiver-Stokes system with finite element method. In this system a horizontal channel is branched into two identical and symmetric branches with the walls of the channels assigned several different wettability values. The studied scenarios consider a blob of one phase initially encompassed by the other phase. When an applied pressure difference induces flow, it is found that the motion of the blob in the two branches is significantly influenced by the wettability conditions at the channel walls. For the scenarios in which symmetric wettability configurations are applied, the blob divides equally among the two branches. For all the other scenarios in which the wettability configurations are asymmetric, the blob splits unequally. Comparisons between the different scenarios are performed in terms of the volume of the blob in each branch to investigate the percentage of the blob volume moving in each branch. In this work it is demonstrated that even though the pressure gradient is the same among the two symmetric branches, the phases partition differently when asymmetric wettability conditions are applied. The significance of this work may be that it provides evidences that relative permeability (a concept that has been introduced in the study of multiphase flow in porous media) may be more complex than just a mere scalar quantity function of saturation. It also highlights the importance of including the effects of wettability conditions in capillary pressure relationships

Keywords: two-phase immiscible flow, coupled Navier-Stokes and Cahn-Hillard, moving contact line, finite element method.

Introduction

Porous media involve in addition to its complex internal structure, complex texture properties that could influence the motion of flowing fluids and dissolved materials. That is naturally occurring porous media involve several organic and inorganic materials which have very different affinities to the phases of flowing fluids. While the organic part of the soil has affinity to organic-based fluids like oil, inorganic and mineral rocks largely have affinities to water-based fluids. In other words, fluids moving in such formations will move under the influence of such affinity conditions in addition to the imposed pressure gradient. Furthermore, the displacement of one fluid by another immiscible with it provides a class of flow system that is complex to treat particularly if both fluids have different affinity to the confining pore surface materials. This situation can be found in many engineering applications including the displacement of oil with water or carbon dioxide, etc. The framework that is usually adapted to studying these multiphase systems in porous media is generally based on the continuum hypothesis in which overlapping continua of the phases interact with each other. In this framework, macroscopic variables represent continuous functions of space and time [e.g., 1-7]. Within this framework all the complexities of multiphase systems in porous media have been, in practice, lumped into only one parameter; called relative permeability, which has been assumed, primarily, function of saturation of respective phases. It has, however, been recognized the complex dependence of relative permeability on other factors (e.g., the wettability conditions of porous media surfaces). However, such dependence has always been incorporated into the saturation dependence. This implies that, for identical porous media structure we could have different relative permeability functions only because of differences of texture's wettability. In general, the role of wettability on the flow characteristics of multiphase system in porous media is not very well comprehended. It is our belief that, any success in adopting a macroscopic description to the problem of flow of multiphase system in porous media is very much provisional to our success in accurately describing fluid movement at the fluid continuum scale (i.e., at pore scale). That is, still much need to be done to accurately solve this problem, particularly on how to define the boundary conditions near the contact line of the fluid-fluid interface when they intersect the solid wall, where the traditional no-slip boundary condition may not be valid. For decades it has been a common practice in continuum fluid mechanics to consider a no-slip condition at the fluid-solid interface. However, this assumption results in an inaccurate modeling for the moving contact line problem. Several research works pointed out that, conventional theories of fluid mechanics fail to capture such slippage, which have been identified as the moving contact line problem [e.g., 8-16]. A few approaches have been proposed for which a good list can be found in He and Wang [17]. For example Qian et al. [18] suggested the need to using the generalized Navier boundary condition (GNBC) to handle the moving contact line problem. With the generalized Navier boundary condition, relative slippage between the fluids and the solid surface is allowed and is assumed proportional to the sum of tangential viscous stresses and the uncompensated

Young stress. In their framework, the coupled system of Cahn–Hilliard (CH) equations and the Navier–Stokes (NS) equations along with the GNBC provide a natural framework to dealing with the contact line problem. Their numerical results obtained using this framework show very good quantitative agreement with the results from the Molecular Dynamics (MD) simulations.

In this work, we investigate the influence of wettability conditions on the flow of two phase system in a branched Y-shaped channel under the effect of pressure difference. The aim is to show how wettability can entail the direction of the flow of the phases. This is extremely important in applications in which one fluid displaces another immiscible with it, e.g., in oil production. However, as explained earlier, because of the complexity of the internal structure of porous media, we consider a simple geometry at the pore scale. We consider the problem of flow divide of two immiscible fluids in a small channel. This geometry is a simplified version of flow branching in pore space within porous media and the different wettability conditions represent the heterogeneity of porous media texture. We would like to highlight the fact that splitting of phases among identical branching may be different according to their wettability characteristics. That is even if the pressure difference along the two branches is identical, yet the flow of the phases may be different along the two branches. The significance of this work is related to the idea that even if the medium may be isotropic and homogeneous with respect to the absolute permeability, a condition which entails the flux and the pressure gradient vectors to be coincident, still the direction of the flow of the two-phase system may be different than the imposed pressure gradient direction as a result of wettability conditions. In other words, the flow of the phases may preferentially select certain routes where the affinity is favorable. It is worth mentioning that Mehrabian et al. [20] numerically investigated wicking through micropores of two-dimensional planar channels with a Y-shaped symmetric bifurcation under the influence of capillary forces. They considered steady Stokes equations coupled with Cahn-Hillard equation with a no slip boundary conditions. Since the flow under capillary forces is usually slow, the interface did not deform much from the nearly spherical shape. In this work, however, we consider the full unsteady Navier-Stokes equations as well as the generalized Navier boundary condition to account for the moving contact line dynamics. In such pressure driven flows, the interface assumes complex configurations as will be apparent later.

1. Physical models

The moving contact line problem, which is related closely to wetting phenomena, occurs where the interface of two immiscible fluids intersects the solid surface. It has been a classical problem in both theoretical and applied research. In Qian et al. [18], the following coupled Cahn-Hilliard and Navier-Stokes system along with the generalized Navier boundary condition (GNBC) is proposed to handle the moving contact line problem.

$$\rho(\frac{\partial \mathbf{u}}{\partial t}+(\mathbf{u}\cdot\nabla)\mathbf{u})=-\nabla p+\eta\Delta\mathbf{u}+\mu\nabla\phi \quad in\ \Omega \tag{1}$$

$$\nabla\cdot\mathbf{u}=0 \quad in\ \Omega \tag{2}$$

$$\frac{\partial\phi}{\partial t}+\mathbf{u}\cdot\nabla\phi=M\Delta\mu \quad in\ \Omega \tag{3}$$

In the above system, $\mathbf{u}=(u_x,u_y)$ is the velocity, p is the pressure, η is the dynamic viscosity, ρ is the mass density, ϕ is the phase field value, M is the phenomenological mobility coefficient, μ is the chemical potential and $\mu=-K\Delta\phi-r\phi+u\phi^3$, $\mu\nabla\phi$ is the capillary force, K, r and u are the parameters that are related to the interface thickness $\xi=\sqrt{K/r}$, the interfacial tension $\gamma=2\sqrt{2}r^2\xi/3u$, and the two homogeneous equilibrium phases $\phi_\pm=\pm\sqrt{r/u}$ ($=\pm1$ in the paper). In the paper, the effects of the wettability are investigated, and constant mass density ρ and dynamic viscosity η are assumed.

With the generalized Navier boundary condition, a slip velocity is imposed along the tangential direction of the solid surface and evaluated as

$$\beta u_\tau^{slip} = -\eta(\partial_n u_\tau + \partial_\tau u_n) + L(\phi)\partial_\tau \phi \quad on\ \Gamma_{slip} \tag{4}$$

where $L(\phi) = K\partial_n \phi + \partial \gamma_{\omega f}(\phi) / \partial \phi$, $\gamma_{\omega f}(\phi) = -\frac{1}{2}\gamma \cos\theta_s \sin(\frac{\pi}{2}\phi)$, θ_s is the static contact angle, $u_n = \mathbf{u} \cdot \mathbf{n}$ and $u_\tau = \mathbf{u} \cdot \boldsymbol{\tau}$ are the normal and tangent velocity on the slip boundary respectively, where $\mathbf{n}$ and $\boldsymbol{\tau}$ are the unit normal and tangent vectors at the slip boundary, respectively, β is the slip coefficient.

For the Cahn-Hilliard equation, Eq. (3), the following relaxation equation is imposed along the solid surface.

$$\frac{\partial \phi}{\partial t} + u_\tau \partial_\tau \phi = -\Gamma(L(\phi)) \quad on\ \Gamma_{slip} \tag{5}$$

Here, Γ is a phenomenological parameter and should be positive. The following non-penetration boundary conditions are also used on the solid boundary.

$$u_n = 0, \quad \partial_n \mu = 0 \quad on\ \Gamma_{slip} \tag{6}$$

And also, the Dirichlet pressure boundary condition is applied on the inlet and outlet boundary.

$$p = p(\mathbf{x}) \quad on\ \Gamma_{inlet} \cup \Gamma_{outlet} \tag{7}$$

Following Qian [18], Gao and Wang [21], and Bao et al. [22], the dimensionless equations for the coupled system are obtained by scaling length by the reference length L_0 , velocity by the reference velocity V and the time by L_0 / V .

$$R(\frac{\partial \mathbf{u}}{\partial t}+\mathbf{u}\cdot\nabla\mathbf{u})=-\nabla p+\Delta\mathbf{u}+\lambda\mu\nabla\phi \quad in\ \Omega \tag{8}$$

$$\nabla\cdot\mathbf{u}=0 \quad in\ \Omega \tag{9}$$

$$\frac{\partial\phi}{\partial t}+\mathbf{u}\cdot\nabla\phi=L_d\Delta\mu \quad in\ \Omega \tag{10}$$

$$\mu=-\varepsilon\Delta\phi-\frac{1}{\varepsilon}(\phi-\phi^3) \quad in\ \Omega \tag{11}$$

Here, ε is the ratio between interface thickness ξ and reference length L_0. The boundary conditions along the slip boundary are reformulated as follows accordingly.

$$\frac{u_\tau^{slip}}{L_s}=-(\partial_n u_\tau+\partial_\tau u_n)+\lambda L(\phi)\partial_\tau\phi \quad on\ \Gamma_{slip} \tag{12}$$

$$\phi_t+u_\tau\partial_\tau\phi=-V_s L(\phi) \quad on\ \Gamma_{slip} \tag{13}$$

$$u_n=0, \quad \partial_n\mu=0 \quad on\ \Gamma_{slip} \tag{14}$$

where $L(\phi)=\varepsilon\partial_n\phi-\frac{\sqrt{2}}{6}\pi\cos\theta_s\cos\left(\frac{\pi}{2}\phi\right)$. In the above equations, six dimensionless parameters are introduced and they are $L_d=3M\gamma/2\sqrt{2}VL_0^2$, $R=\rho VL_0/\eta$, $\lambda=3\gamma/2\sqrt{2}\eta V$, which is inversely proportional to the capillary number $C_a=\eta V/\gamma$, $V_s=K\Gamma/V$, which is the ratio of $K\Gamma$ to V, $L_s=\eta/\beta L_0$,which is the ratio of slip length $l_s=\eta/\beta(\phi)$ to L_0 and ε.

2. Numerical solution

The numerical solution of the governing equations describing the flow of multiphase systems have been the topic for extensive research because of its practical importance [e.g., 22-25]. More details about the current modeling approach can be found in Bao et al. [26]. For the sake of completion, however, we highlight the essence of the numerical scheme used in this work. A second order finite element method is used to solve the coupled system numerically. Here, the employed numerical scheme is presented in a brief way for completeness. In the paper, the coupled Cahn-Hilliard and Navier-Stokes system is solved in a decoupled way to simplify the simulation. For the Cahn-Hilliard equations, a second order semi-implicit temporal discretization with a convex splitting scheme is employed. In this scheme, a stabilizing parameter s is introduced. It has been shown that when $s \geq (3M^2 - 1)/2$, where $M = \sup_{\mathbf{x}\in\Omega}\{|\phi|\}$, the employed convex splitting scheme is unconditionally stable, Gao and Wang [21]. In the paper, $s = 2.5$ is chosen in the simulations. For the Navier-Stokes equations, a linearized semi-implicit scheme is used to avoid the non-linear iterations.

The second order of the temporal scheme for the system is formulated as follows.

$$\mu^{n+1} = -\varepsilon\Delta\phi^{n+1} + \frac{s}{\varepsilon}\phi^{n+1} - \frac{2(1+s)}{\varepsilon}\phi^{n} + \frac{(1+s)}{\varepsilon}\phi^{n-1} + \frac{2(\phi^{n})^{3}}{\varepsilon} - \frac{(\phi^{n-1})^{3}}{\varepsilon} \tag{15}$$

$$\frac{3\phi^{n+1} - 4\phi^{n} + \phi^{n-1}}{2\delta t} + 2\mathbf{u}^{n}\cdot\nabla\phi^{n+1} - \mathbf{u}^{n-1}\cdot\nabla\phi^{n} = L_d\Delta\mu^{n+1} \tag{16}$$

$$R(\frac{3\mathbf{u}^{n+1} - 4\mathbf{u}^{n} + \mathbf{u}^{n-1}}{2\delta t} + 2\mathbf{u}^{n}\cdot\nabla\mathbf{u}^{n+1} - \mathbf{u}^{n-1}\cdot\nabla\mathbf{u}^{n}) - \Delta\mathbf{u}^{n+1} + \nabla p^{n+1} = \lambda\mu^{n+1}\nabla\phi^{n+1} \tag{17}$$

$$\nabla\cdot\mathbf{u}^{n+1} = 0 \tag{18}$$

And on the slip boundary,

$$\frac{3\phi^{n+1} - 4\phi^{n} + \phi^{n-1}}{2\delta t} + 2u_{\tau}^{n}\partial_{\tau}\phi^{n} - u_{\tau}^{n-1}\partial_{\tau}\phi^{n-1} = -V_s L(\phi^{n}) \tag{19}$$

$$\frac{(u_{\tau}^{slip})^{n+1}}{L_s} = \lambda L(\phi^{n+1})\partial_{\tau}\phi^{n+1} - (\partial_n u_{\tau} + \partial_{\tau} u_n)^{n+1} \tag{20}$$

$$u_n^{n+1} = 0, \quad \partial_n\mu^{n+1} = 0 \tag{21}$$

Here, $L(\phi^{n+1}) = \varepsilon\partial_n\phi^{n+1} - 2\times\frac{\sqrt{2}}{6}\pi\cos\theta_s\cos\left(\frac{\pi}{2}\phi^{n+1}\right) + \frac{\sqrt{2}}{6}\pi\cos\theta_s\cos\left(\frac{\pi}{2}\phi^{n}\right)$.

In the paper, the P2-P0 mixed finite elements space pair is used to discretize the Navier-Stokes equations and P1-P1 space pair is used to discretize the Cahn-Hilliard equations. Both space pairs are stable because they satisfy the inf-sup stable condition [27]. For the Cahn-Hilliard equations, with P1-P1 space pair, the following conservation law is also fulfilled, [28], for the computational domain without inflow and outflow.

$$\int_\Omega \phi_h^m d\mathbf{x} \equiv \int_\Omega \phi_h^0 d\mathbf{x} \quad for\ m \geq 1 \tag{22}$$

For the Naiver-Stokes equations, with the $P_2 - P_0$ space pair, the accuracy of the velocity is second order and the pressure approximation is of first order.

The following finite element spaces are defined to discretize the coupled system spatially.

$$M_h = \{q_h \in L_0^2(\Omega); q_h\big|_K \in P_0(K)\}$$

$$U_h = \{v_h \in C^0(\bar{\Omega}); v_h\big|_K \in P_2(K)\}$$

$$W_h = \{w_h \in C^0(\bar{\Omega});\ w_h\big|_K \in P_1(K)\}$$

where Ω is the computational domain and $L_0^2(\Omega) = \{v \in L^2(\Omega);\ \int_\Omega v d\mathbf{x} = 0$.

The weak formulation for the Cahn-Hilliard equations with the GNBC boundary condition is defined as follows, find $(\phi_h, \mu_h) \in W_h \times W_h$, such that, for $\forall w_h \in W_h$

$$(\frac{3\phi_h^{n+1} - 4\phi_h^n + \phi_h^{n-1}}{2\delta t}, w_h) + (2\mathbf{u}_h^n \cdot \nabla\phi_h^{n+1}, w_h) - (\mathbf{u}_h^{n-1} \cdot \nabla\phi_h^n, w_h) = -L_d(\nabla\mu_h^{n+1}, \nabla w_h) \tag{23}$$

$$
\begin{aligned}
(\mu_h^{n+1}, w_h) &= \varepsilon(\nabla\phi_h^{n+1}, \nabla w_h) + \frac{s}{\varepsilon}(\phi_h^{n+1}, w_h) + \Big(-\frac{2(1+s)}{\varepsilon}\phi_h^n + \frac{(1+s)}{\varepsilon}\phi_h^{n-1} + \frac{2(\phi_h^n)^3}{\varepsilon} - \frac{(\phi_h^{n-1})^3}{\varepsilon}, w_h\Big) \\
&+ \frac{1}{V_s}\left[\left\langle \frac{3\phi_h^{n+1} - 4\phi_h^n + \phi_h^{n-1}}{2\delta t}, w_h \right\rangle_{\Gamma_{slip}} + \left\langle 2u_\tau^n \partial_\tau \phi_h^n - u_\tau^{n-1}\partial_\tau \phi_h^{n-1}, w_h \right\rangle_{\Gamma_{slip}}\right] \\
&+ \left\langle -2\times\frac{\sqrt{2}}{6}\pi\cos\theta_s\cos\left(\frac{\pi}{2}\phi_h^n\right) + \frac{\sqrt{2}}{6}\pi\cos\theta_s\cos\left(\frac{\pi}{2}\phi_h^{n-1}\right), w_h \right\rangle_{\Gamma_{slip}}
\end{aligned}
\tag{24}
$$

The finite element discretization for the Navier-Stokes equations with the GNBC is defined as follows, find $(\mathbf{u}_h, p_h) \in (U_h)^2 \times M_h$, where $\mathbf{u}_h = (u_x, u_y)$, such that, for $\forall(\mathbf{v}_h, q_h) \in (U_h)^2 \times M_h$

$$
\begin{aligned}
&R\Big(\frac{3\mathbf{u}_h^{n+1} - 4\mathbf{u}_h^n + \mathbf{u}_h^{n-1}}{2\delta t}, \mathbf{v}_h\Big) + 2R(\mathbf{u}_h^n \cdot \nabla \mathbf{u}_h^{n+1}, \mathbf{v}_h) - R(\mathbf{u}_h^{n-1} \cdot \nabla \mathbf{u}_h^n, \mathbf{v}_h) + (\nabla \mathbf{u}_h^{n+1}, \nabla \mathbf{v}_h) - (p_h^{n+1}, \nabla \cdot \mathbf{v}_h) \\
&+ < \frac{1}{L_s} u_\tau^{n+1}, v_h >_{\Gamma slip} = \lambda(\mu_h^{n+1} \nabla \phi_h^{n+1}, \mathbf{v}_h) + < (\lambda L(\phi_h^{n+1})\partial_\tau \phi_h^{n+1}, v_h >_{\Gamma_{slip}} - (< P_2, v_h >_{\Gamma_{outlet}} - < P_1, v_h >_{\Gamma_{inlet}})
\end{aligned}
\tag{25}
$$

$$
(\nabla \cdot \mathbf{u}_h^{n+1}, q_h) = 0 \tag{26}
$$

Based on the above discretization equations, two linear systems are obtained for the Cahn-Hilliard equations and Navier-Stokes equations respectively, and UMFPACK Davis [29], an efficient direct linear solver based on the sparse LU factorization, is used to solve the linear systems. Since we solve the coupled system in a decoupled way, mild CFL time constriction is introduced. More detailed discussions on the numerical methods, accuracy analysis, and the physical models employed can be found in [18, 21, and 26].

3. Branching and wetting scenarios

In this work, we consider flow branching among two identical channels the walls of which are having different affinities to the flowing fluids. The two branches considered in this work make an angle α of 30° with the horizontal direction. Figure1 shows a schematic diagram for the computational domain. As shown in Fig. 1, the horizontal channel spans a dimension of $[x,y] \in [-2.0,0.0] \times [-0.1,0.1]$

with two identical branches. The coordinates in x direction of the initial location of the two interfaces are -1.5 and -0.5, respectively. Several wetting scenarios are considered for the walls of the channels. The wetting conditions are defined in this work with respect to the static contact angle $\vartheta_s$between the fluid and the solid. In Fig. 2, the wall is wetting to the blue phase if $\vartheta < 90$ and non-wetting if $\vartheta > 90$. In this work we consider a blob of one fluid completely filling the channel and surrounded by the other fluid forming two contact lines.

In this work, we consider flow branching among two identical channels the walls of which are having different affinities to the flowing fluids. The two branches considered in this work make an angle α of 30° with the horizontal direction. Fig. 1 shows a schematic diagram for the computational domain. Several wetting scenarios are considered for the walls of the channels. The wetting conditions are defined in this work with respect to the static con- tact angle ϑ_s between the fluid and the solid. In Fig. 2, the wall is wetting to the blue phase if $\vartheta < 90$ and non-wetting if $\vartheta > 90$. In this work we consider a blob of one fluid completely filling the channel and surrounded by the other fluid forming two contact lines. As shown in Fig. 1, the horizontal channel spans a dimension of $[x,y] \in [-2.0,0.0] \times [-0.1,0.1]$ with two identical branches. The coordinates in x direction of the initial location of the two interfaces are -1.5 and -0.5, respectively. A triangular mesh system is used with the number of elements used in the simulation on the order of 3×10^4 . In order to build confidence in the used density of the mesh, a convergence test is carried out for one of the scenarios with different resolutions. Three mesh resolutions have been considered similar to that conducted in [26]. The following parameters are set constant during the course of the different examples; these are $Re = 5.0$, $Ca = 2.5$, $ls = 0.0025$, $\varepsilon = 0.003$, $dt = 0.0001$, $\lambda = 12.0$, $Vs = 200$, $Ld = 0.0005$. The used framework is well documented and several verification examples can be found in [26] . These include: 1) two phase Couette flow in a channel, 2) coalescence of two droplets, 3) evolution of contact line over curved surface, and 4) droplet displacement under shear flow, which provides confidence in the modeling approach.

4. Results and discussions

The scenarios considered in this work represent a two-phase immiscible system filling a branched channel. Initially one phase (colored in red) is totally encompassed by the other phase (colored in blue) and the system is forced to flow under the effect of pressure difference. The wettability conditions at the solid walls are predefined according to the following convention, the letter E to defines the case in which the static contact angle is 90°, the letter W to define a wetting fluid with static contact angle 60°, and the letter N to define a non-wetting fluid with static contact angle of 120° and the letter C to define a changing contact angle. In order to assess the effect of wettability conditions on the flow branching characteristics of this two-phase system, we define the volume of the two phases (ϕ_+ for the red phase and ϕ_- for the blue phase) in each branch at a given time as

$$\left| \int_{A_{branch}} \phi_{\pm}(\mathbf{x},t)\, d\mathbf{x} \right| \tag{26}$$

This parameter is a measure of the amount of each phase in the two branches. Apparently when the wettability conditions are symmetric along the system, both phases will divide equally into the two branches. Figure 3-a-c shows the splitting among the two channels and it is easy to see that the flow is identical in the two branches. As a result of the different wettability configurations in the different scenarios, different shapes of the interface are observed, while the volumes of the red phase are the same due to the symmetric configurations. On the other hand, when the wettability conditions among the two branches are nonsymmetrical, the phases are divided unequally with the amount of each phase in the two branches significantly influenced by the magnitude of the contact angle and the patterns of wettability conditions at the different channel walls. To highlight this effect, several scenarios have been considered including; EEEECC, ECEECC, etc. In the first scenario, namely the EEEECC, the walls of the horizontal channel as well as that of the top branch are assigned a neutral wettability condition (i.e., contact angle of 90^o) while that of the bottom branch are changing from highly wetting to highly non wetting conditions (i.e., contact angle spanning magnitudes between 20^o to 160^o). Interesting patterns are observed as manifested in Fig. 4-a-h which shows snap shots of the phases configurations. It is clear from this figure that both the configuration and the amount of the red phase in both branches are different. When the static contact angle of the bottom branch has been set to 20^o, i.e., highly wetting conditions, the red phase preferentially moves towards the bottom branch, Fig. 4-a. Furthermore, two prolonged tails are formed for the red phase as a consequence of the highly wetting conditions of the walls. It is also noticed that the bottom most tail is longer than the top one in the bottom branch which is a consequence of the fact that the red phase reaches the bottom wall earlier than the top wall. When the contact angle of the bottom branch has been set to 40^o, similar pattern is observed, Fig. 4-b. The long tails, however, are shorter as a manifestation of the less wettability. As the contact angle of the bottom branch increases (i.e., the walls become less wetting) the volume of the red phase decreases as shown in Figs. 4-c, d. Furthermore, the tail of the red phase in the bottom branch shrinks significantly compared with the previous two cases. When the walls of the bottom branch are non-wetting (i.e., the contact angle is larger than 90^o) the volume of the red phase moving in the bottom branch becomes even smaller as shown in Figs. 4-e-h. Furthermore for the highly non-wetting scenario the red phase is detached from the wall as shown in Fig. 4-h. Figure 5 shows the evolution of the volume of the red phase in the bottom branch with time for different wettability conditions of the bottom branch. It is clear that when the walls of the bottom branch are wetting with respect to the red phase that the volume divides more towards the bottom branch. Furthermore, for the highly wetting scenarios, the volume of the red phase in the bottom branch takes longer time to drop to zero because of the longer tail. Figure 6 shows the volume of the red phase in the two branches with respect to the different contact angle of the bottom branch. It is clear that the volume of the red phase in the bottom channel decreases with the increase in the contact angle while it increases in the top channel.

The second investigated scenario considers the bottom wall of the horizontal channel as well as the walls of the bottom branch changing (i.e., ECEECC). Figure 7 shows the different configurations of the two phases associated with this scenario. It is clear that for the highly wetting scenarios the tail along the bottom walls is much longer compared with the previous scenario, Fig. 7-a-c. Even for moderately wetting conditions (e.g., static contact angle of 60^o) that there exists a longer tail at the bottom walls as compared with the previous scenario. When the contact angle is larger than 90^o, similar patterns to the previous scenario are observed as depicted in Fig. 7-e-h. Figure 8 shows the volume of the red phase in the two branches with the contact angle. It is easy to see that the red phase splits more in this scenario compared with the previous scenario. In other words more of the red phase volume splits towards the bottom branch particularly when the contact angle is smaller.

In the third scenario the top branch has been assigned a wetting condition and the bottom branch a varying wettability (i.e., EEWWCC) with contact angle changing between 20^o to 160^o. This scenario is clearly similar with the first scenario but with the top branch having much more affinity to the red phase as oppose to being neutral as in the first scenario. In this case the configuration of the red phase in the bottom branch is almost similar to that in the first scenario but the volume of the red phase is apparently different, Fig. 9-a-h. This is because more of the red phase is now moving in the top branch because of the relatively favorable wettability. This can also be seen on comparing the volume of the red phase in the two branches with contact angle as depicted in Fig. 10. In this figure it is clear that the red phase splits less when the contact angle is less than 60^o which is the condition of the top branch.

In the last two scenarios, it has been assumed that the wetting and non-wetting conditions are such that the sum of the contact angle is 180^o. In the first of the two scenarios, EENNWW, both the top and the bottom branches has been set to this rule. As an example if the contact angle of the bottom branch to the red phase is set to 40^o the top branch is assigned a contact angle of 140^o. It is clear that the maximum split occurs when the contact angle of the bottom branch is the smallest and that of the top branch is the highest and indeed this is what is observed as depicted in Fig. 11-a-d. This can also be seen on comparing the volume of the red phase in each branch as depicted in Fig. 12.

The last scenario denoted as NWNNNW is also based on the predefined rule that N+W=180^o. It is clear that again more of the red phase splits towards the bottom branch. There exists a longer tail due to the effect of the wettability of the bottom wall of the horizontal channel. Furthermore the red phase detaches the top wall of the bottom channel which has been assigned a non-wetting condition, Fig 13-a-d. This can also be anticipated on comparing the volume of the red phase with the contact angle as depicted in Fig. 14.

From the previously mentined examples it is clear that as long as there is no symmetry in the wettability conditions among the sides of the branched channel, the phases divides unequally among the two branches. Figure 15 shows a comparison between the volume of the red phase in both channels under the different wettability scenarios. It is clear that the difference in wettability affects the volume of the red phase moving in the two channels. Also some scenarios has larger effect on the split characteristics of this system than others. It is clear that when the wettability conditions are continuous (i.e., with respect to the bottom and/or the top walls of the system) that the phases split the most.

Conclusions

A pore-scale numerical investigation of the problem of flow splitting characteristics of a two-phase system among two symmetric branches of a horizontal channel is introduced. The two branches are making an angle of 30^o with the horizontal direction. In this work we highlight the fact that even if the pressure gradient is identical among the two branches, the phases may split differently according to the wettability conditions. Therefore, at porous media continuum scale, in which the complexity of the flow of a two-phase system has been lumped into a single scalar parameter depending on saturation (the so called relative permeability), one may need to include wettability condition. Different wetabbility conditions of the walls of the main channel and the two branches are considered. It has been shown that when the wettability conditions of the channel walls are symmetric, that the phases split symmetrically among the two branches. When the wettability are not symmetric, the phases split unequally. It has also been found that the split divide is more pronounced when the wettability conditions are continuous (i.e., either the bottom walls or the top walls are both wetting)

References

[1] S. Whitaker, Advances in the Theory of Fluid Motion in Porous Media, Indust. Eng. Chem. Fund., vol. 61, pp.14–28, 1969.

[2] S. M., Hassanizadeh, and W. Gray, General conservation equations for multi-phase systems 1. averaging procedure, Advances in Water Resources 2: 131–144, 1979.

[3] S. M., Hassanizadeh, and W. Gray, General conservation equations for multi-phase systems 2. mass, momenta, energy and entropy equations, Advances in Water Resources 2: 191–208, 1979.

[4] S. M., Hassanizadeh, and W. Gray, General conservation equations for multi-phase systems 3. constitutive theory for porous media, Advances in Water Resources 3: 25–40, 1980.

[5] A. Salama and P. J. Van Geel, Flow and Solute Transport in Saturated Porous Media: 1. The Continuum Hypothesis, J. Porous Media, 11, 4, 403-413, 2008

[6] A. Salama and P. J. Van Geel, Flow and Solute Transport in Saturated Porous Media: 2. Violating the Continuum Hypothesis, J. Porous Media, 11, 5, 421-441, 2008.

[7] M.F. El-Amin, A. Salama, and S. Sun, Solute Transport with Chemical Reaction in Single and Multi-Phase Flow in Porous Media, in Mass Transfer in Multiphase Systems and its Applications, ed. M.F. El Amin, 2011.

[8] C. Huh and S.G. Mason, The steady movement of a liquid meniscus in a capillary tube. J. Fluid Mech., 81:401-419, 1977.

[9] E.B. Dussan, V., On the spreading of liquids on solid surfaces: static and dynamic contact lines. Ann. Rev. Fluid Mech., 11:371-400, 1979.

[10] J.F. Joanny and P.G.de Gennes, A model for contact angle hysteresis. J. Chem. Phys., 81:552-562, 1984.

[11] R.G. Cox, The dynamics of the spreading of liquids on a solid surface. Part 1. Viscous flow. J. Fluid. Mech., 168:169-194, 1986.

[12] J. Koplik, J.R. Banavar, and J.F. Willemsen, Molecular dynamics of poiseuille flow and moving contact lines. Phys. Rev. Lett., 60:1282-1285, 1988.

[13] P.A. Thompson and M.O. Robbins, Simulations of contact-line motion: slip and the dynamic contact angle. Phys. Rev. Lett., 63:766-769, 1989.

[14] P.A. Thompson, W.B. Brinckerhoff, and M.O. Robbins, Microscopic studies of static and dynamic contact angles. J. Adhesion Sci. Tech., 7:535-554, 1993.

[15] H.Y. Chen, D. Jasnow, and J. Vinals, Interface and contact line motion in a two phase fluid under shear flow. Phys. Rev. Lett., 85:1686-1689, 2000.

[16] D. Jacqmin, Contact-line dynamics of a diffuse fluid interface. J. Fluid. Mech., 402:57-88, 2000.

[17] Q. He and X.-Ping Wang, Numerical study of the effect of Navier slip on the driven cavity flow; Z. Angew, Math. Mech, 89, 10, pp. 857 – 868, 2009.

[18] T. Qian, X. P. Wang, and P. Sheng, "Molecular scale contact line hydrodynamics of immiscible flows," Phys. Rev. E 68, 016306, 2003.

[19] T. Qian, C. Wu, S. L. Lei, X.-P. Wang, and P. Sheng, Modeling and simulations for molecular scale hydrodynamics of moving contact line in immiscible two phase flows, Journal of Physics: Condensed Matter 21, 464119 (2009).

[20] H. Mehrabian, P. Gao, and J. J. Feng, Wicking flow through microchannels, Physics of Fluids 23, 122108, 2011.

[21] M. Gao, X.-P. Wang, “A Gradient Stable Scheme for a Phase Field Model for the Moving Contact Line Problem”, J. Computational Physics, 231, 4, pp. 1372-1386, 2012.

[22] B. Lakghomi, F. Taghipour, D. Posarac, A.P. Watkinson, CFD simulation and experimental measurement of droplet deposition and hydrocarbon fouling at high temperatures, Chemical Engineering Journal, 172, 1, 2011, 507-516

[23] K. Sivaguru, K.M. Meera Sheriffa Begum, N. Anantharaman, Hydrodynamic studies on three-phase fluidized bed using CFD analysis, Chemical Engineering Journal, 155, 1–2, 2009, 207-214.

[24] R.J.G. Lopes, R. M. Quinta-Ferreira, CFD modelling of multiphase flow distribution in trickle beds, Chemical Engineering Journal, 147, 2–3, 2009, 342-355

[25] K. Ekambara, R.S. Sanders, K. Nandakumar, J.H. Masliyah, CFD simulation of bubbly two-phase flow in horizontal pipes, Chemical Engineering Journal, 144, 2, 2008, 277-288

[26] K. Bao, Y. Shi, S. Sun, X.-P. Wang, A finite element method for the numerical solution of the coupled cahn-hilliard and Navier-Stokes system for moving contact line problems, J. Computational Physics, 231, 24, pp. 8083-8099, 2012.

[27] F. Xiaobing and A. Prohl, “Error Analysis of a Mixed Finite Element Method for the Cahn-Hilliard Equations”. Numer. Math, 99, 1, pp. 47-84, 2004

[28] F. Xiaobing, Fully discrete finite element approximations of the Navier-Stokes-Cahn-Hilliard diffuse interface model for two phase flows. SIAM J. Numer Anal, 44, 3, pp. 1049-1072, 2006

[29] T. A. Davis, A column pre-ordering strategy for the unsymmetric-pattern multifrontal method, ACM Transactions on Mathematical Software, 30, 2, pp. 165-19, 2004

List of figures

Fig.1Schematic diagram of branching scenarios.

Fig.2 Schematic diagram of one wetting scenario.

Fig. 3 Splitting of the two fluids among the two branches for the symmetric wettability scenarios.

Fig. 4 Different flow configurations of the red phase for different contact angle of the bottom branch for the scenario EEEECC after time= 120 (E: 90^o)

Fig. 5 Volume of the red phase in the bottom branch with time for the different wettability scenarios (EEEECC)

Fig. 6 Volume of the red phase in the two branches for the different contact angle scenarios (EEEECC)

Fig. 7 Different flow configurations of the red phase for different contact angle of the bottom branch for the scenario ECEECC after time= 120 (E: 90^o)

Fig. 8 Volume of the red phase in the two branches for the different contact angle scenarios (ECEECC)

Fig. 9 Different flow configurations of the red phase for different contact angle of the bottom branch for the scenario EEWWCC after time= 120 (E: 90^o, W: 60^o)

Fig. 10 Volume of the red phase in the two branches for the different contact angle scenarios (EEWWCC)

Fig. 11 Different flow configurations of the red phase for different contact angle of the bottom branch for the scenario EENNWW after time= 115 (E: 90^o, N+W: 180^o)

Fig. 12 Volume of the red phase in the two branches for the different contact angle scenarios (EENNWW)

Fig. 13 Different flow configurations of the red phase for different contact angle of the bottom branch for the scenario NWNNNW after time= 105 (N+W: 180^o)

Fig. 14 Volume of the red phase in the two branches for the different contact angle scenarios (NWNNNW)

Fig. 15 Comparison of the volume of the red phase in both channels for different wettability scenarios.

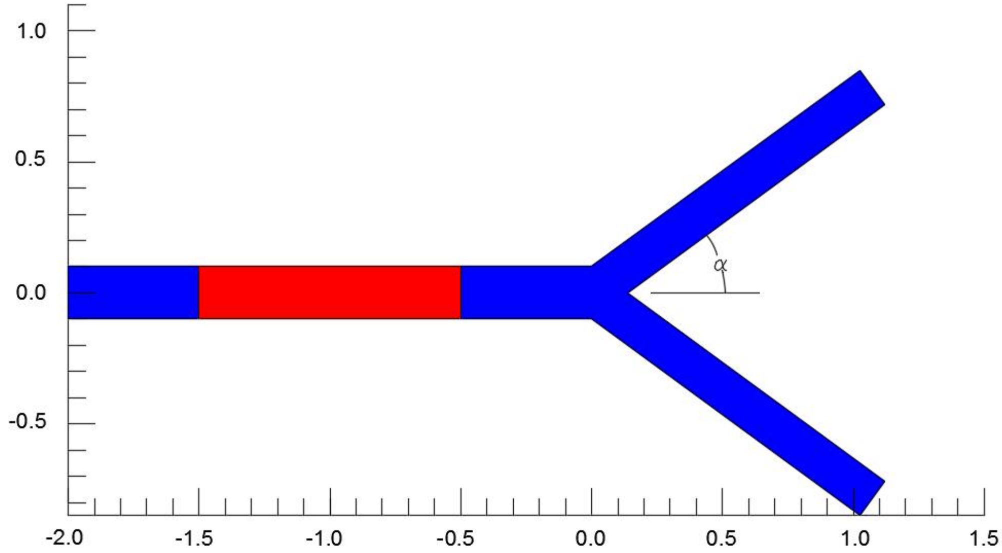

Fig.1 Schematic diagram of branching scenarios.

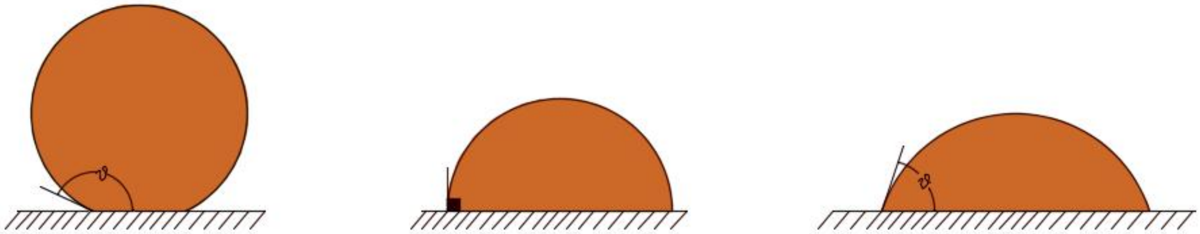

Nonwetting, $\vartheta > 90$ Neutral, $\vartheta = 90$ Wetting $\vartheta < 90$

Fig.2 Different wetting conditions.

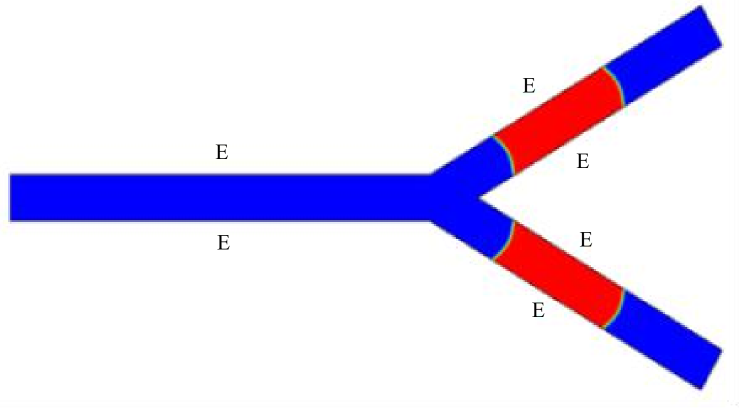

(a) EEEEEE

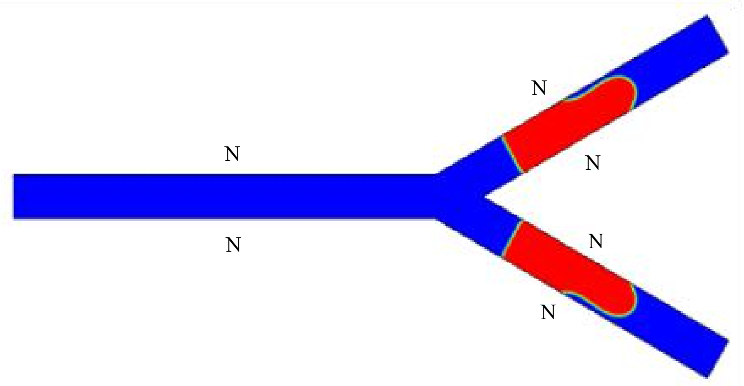

(b) NNNNNN

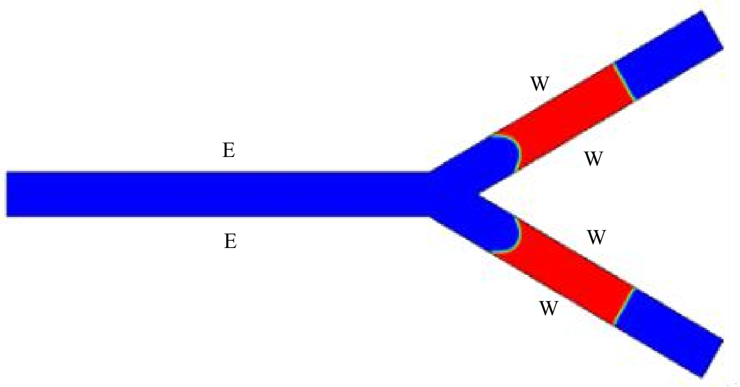

(d) EEWWWW

Fig. 3 Splitting of the two fluids among the two branches for symmetric wettability scenarios.

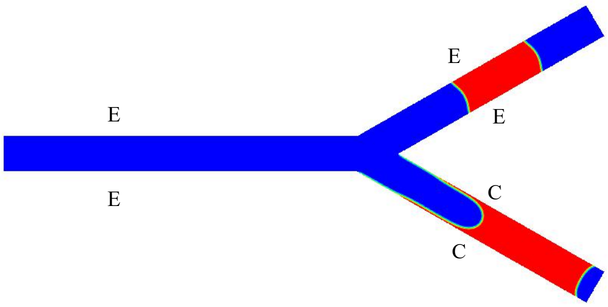

a) C: Angle=20^o Time 120

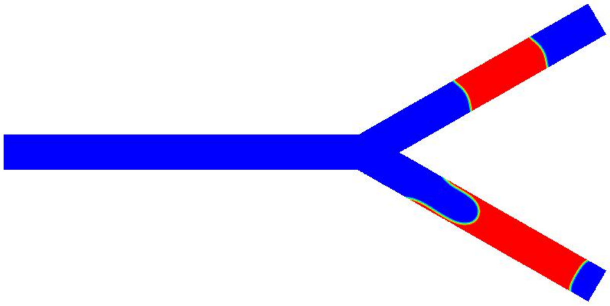

b) C: Angle=40^o

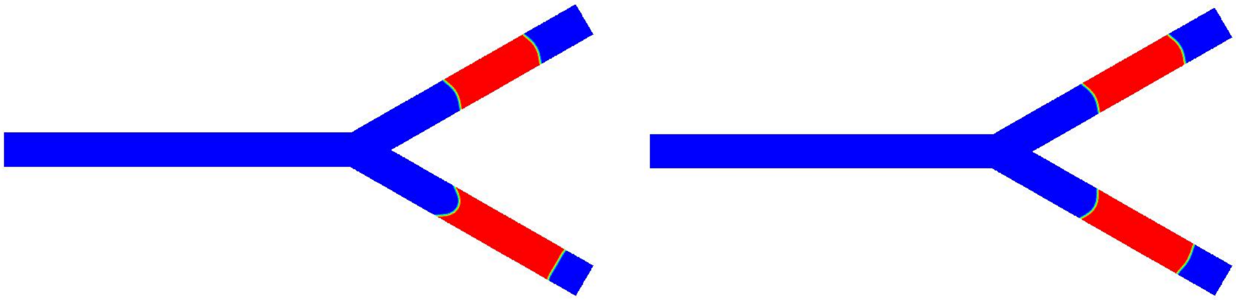

c) C: Angle=60°

d) C: Angle=80°

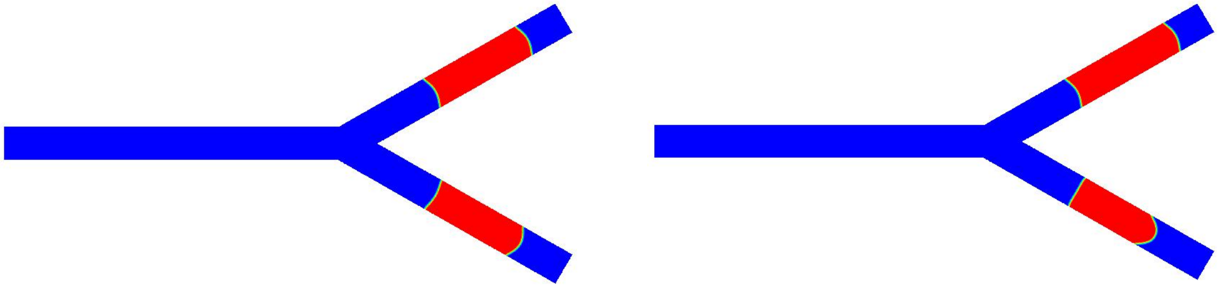

e) C: Angle=100°

f) C: Angle=120°

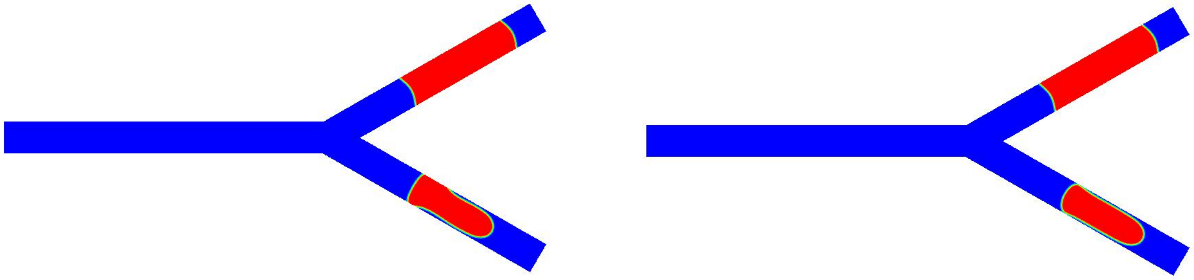

g) C: Angle=140°

h) C: Angle=160°

Fig. 4 Different flow configurations of the red phase for different contact angle of the bottom branch for the scenario EEEECC after time= 120 (E: 90°)

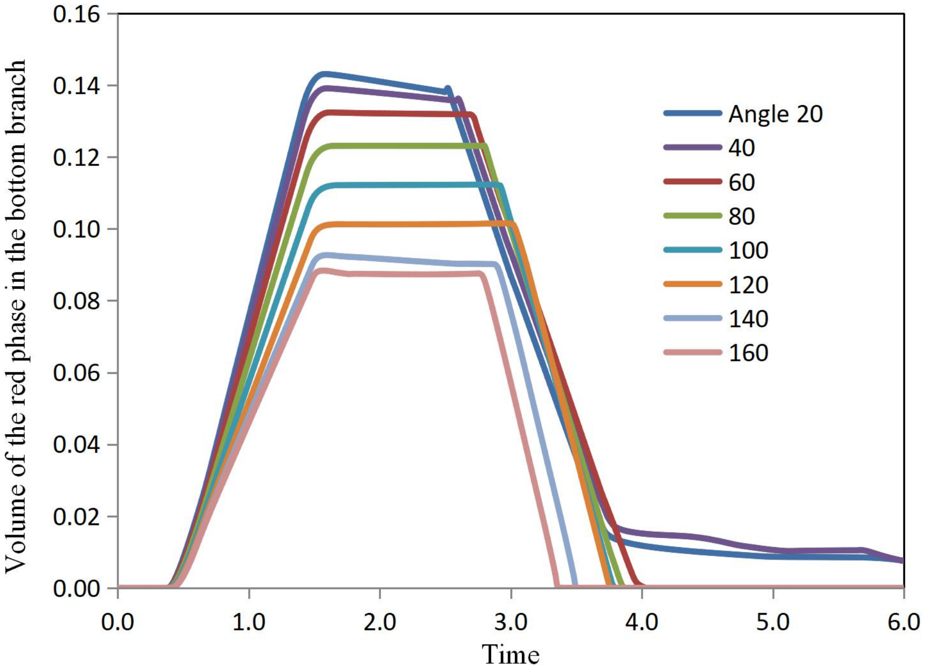

Fig. 5 Volume of the red phase in the bottom branch with time for the different wettability scenarios (EEEECC)

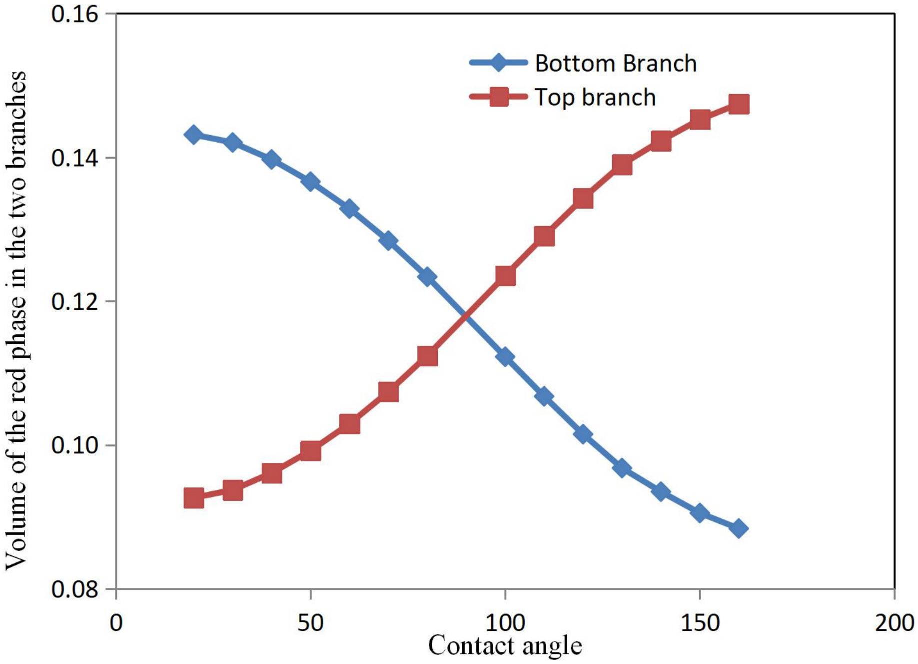

Fig. 6 Volume of the red phase in the two branches for the different contact angle scenarios (EEEECC)

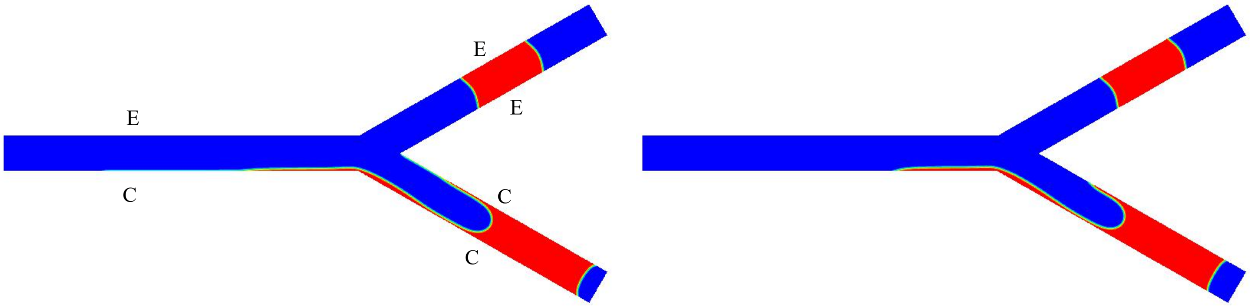

a) C: Angle=20^{o}

b) C: Angle=40^{o}

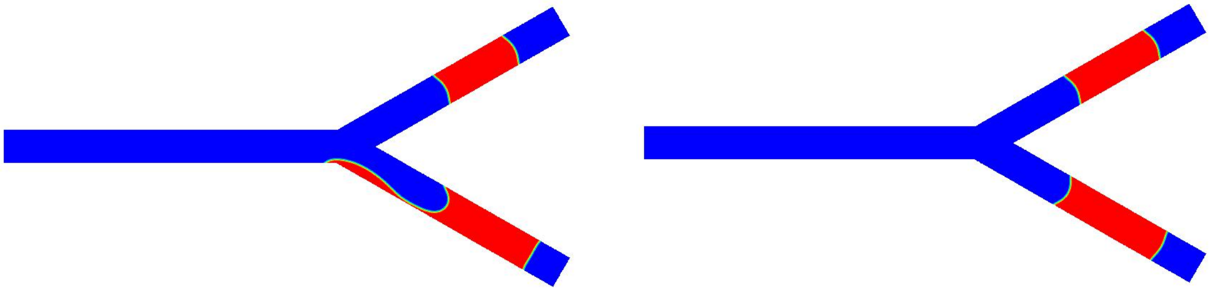

c) C: Angle=60^{o}

d) C: Angle=80^{o}

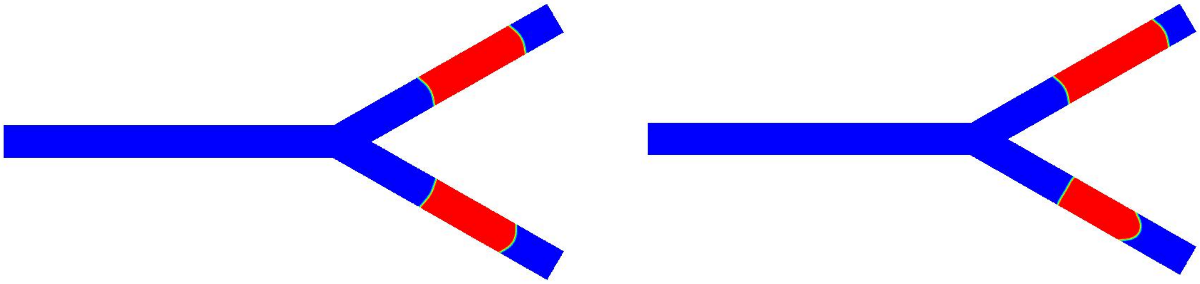

e) C: Angle=100^{o}

f) Angle=120^{o}

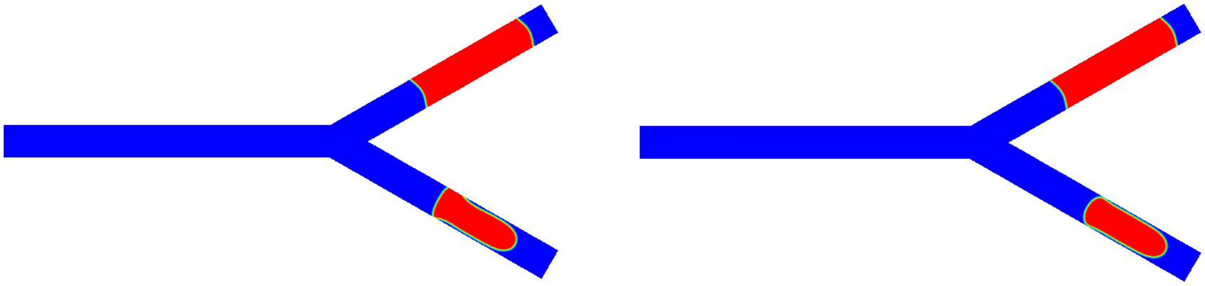

g) C: Angle=140^{o}

h) C: Angle=160^{o}

Fig. 7 Different flow configurations of the red phase for different contact angle of the bottom branch for the scenario ECEECC after time= 120 (E: 90^{o})

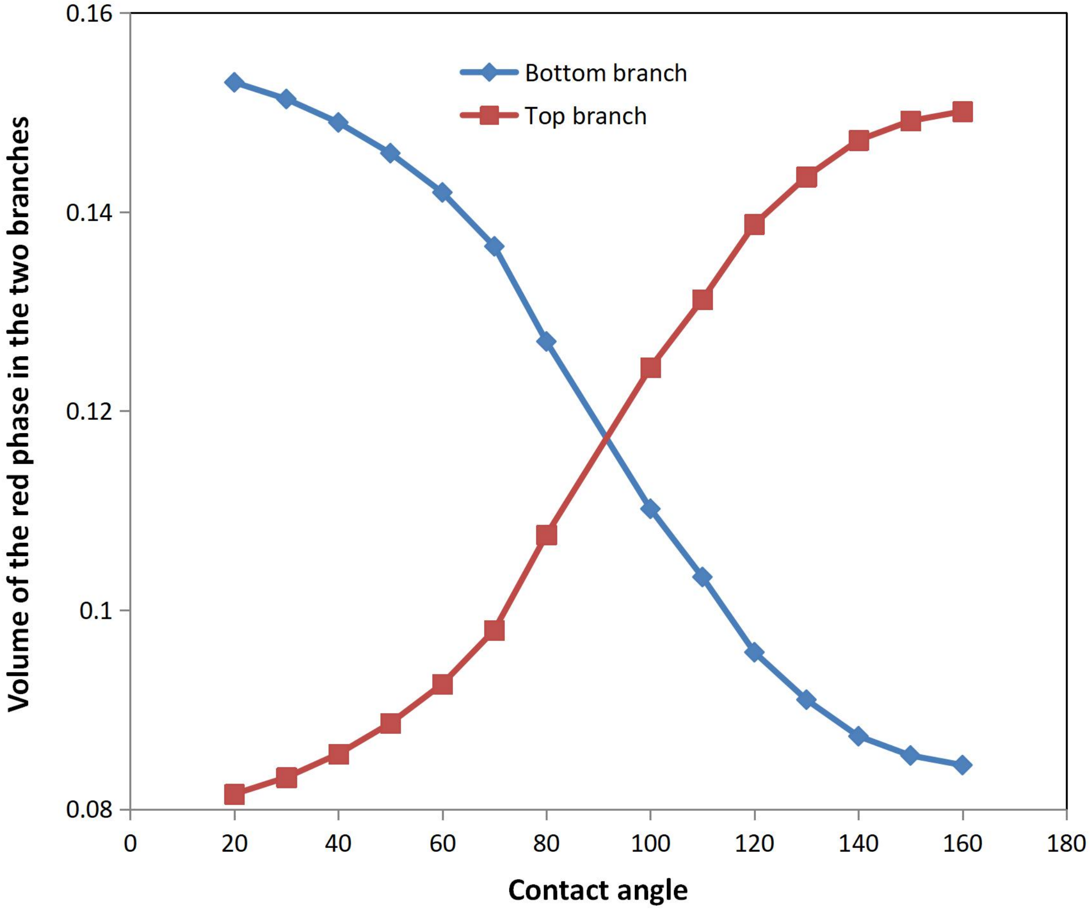

Fig. 8 Volume of the red phase in the two branches for the different contact angle scenarios (ECEECC)

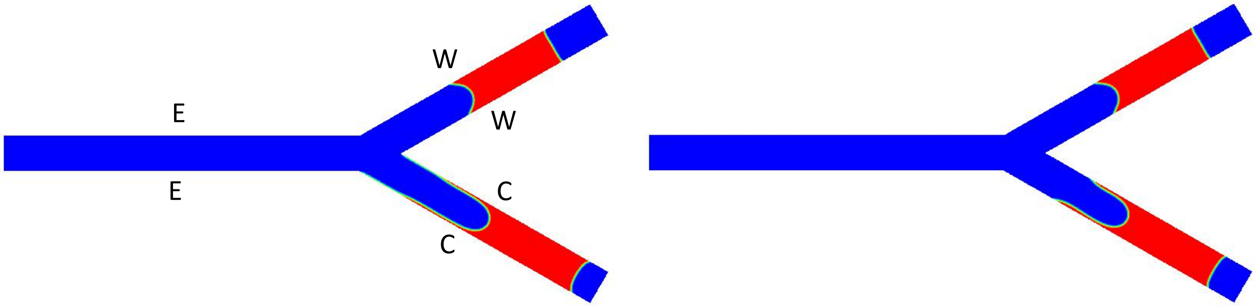

a) C: Angle=20°

b) C: Angle=40°

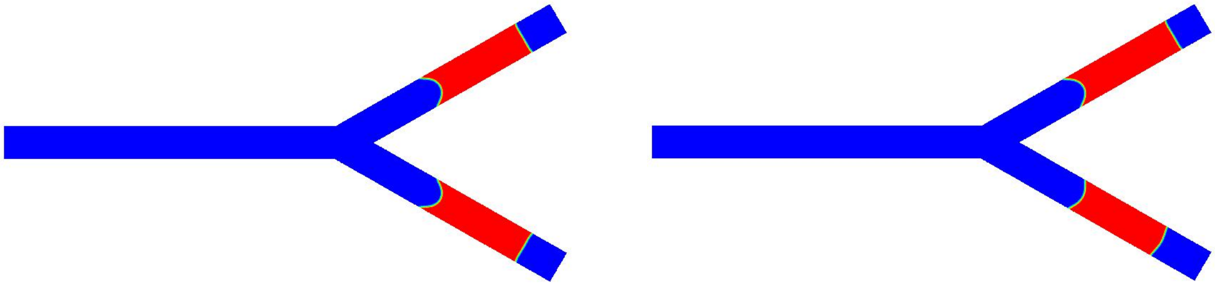

c) C: Angle=60°

d) C: Angle=80°

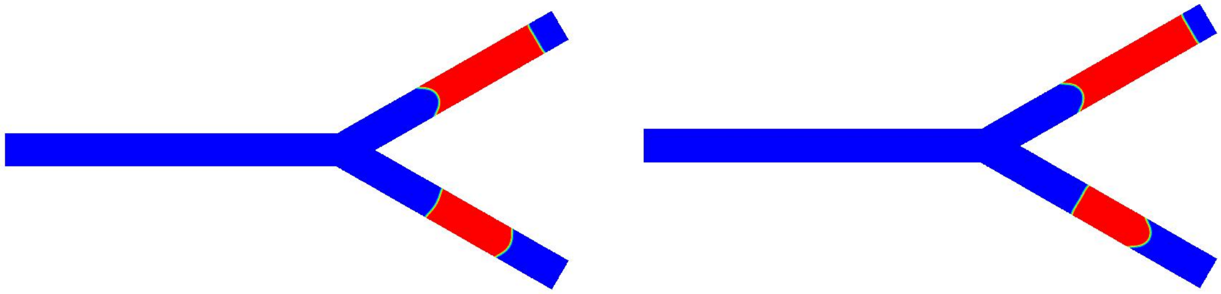

e) C: Angle=100°

f) C: Angle=120°

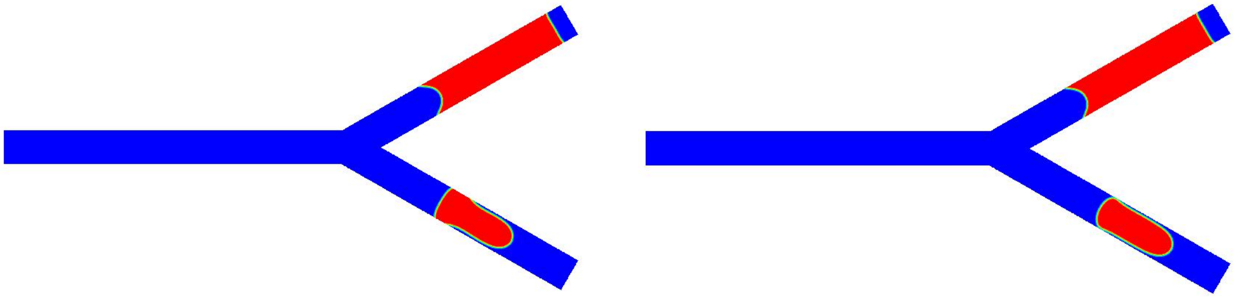

g) C: Angle=140°

h) C: Angle=160°

Fig. 9 Different flow configurations of the red phase for different contact angle of the bottom branch for the scenario EEWWCC after time= 120 (E: 90°, W: 60°)

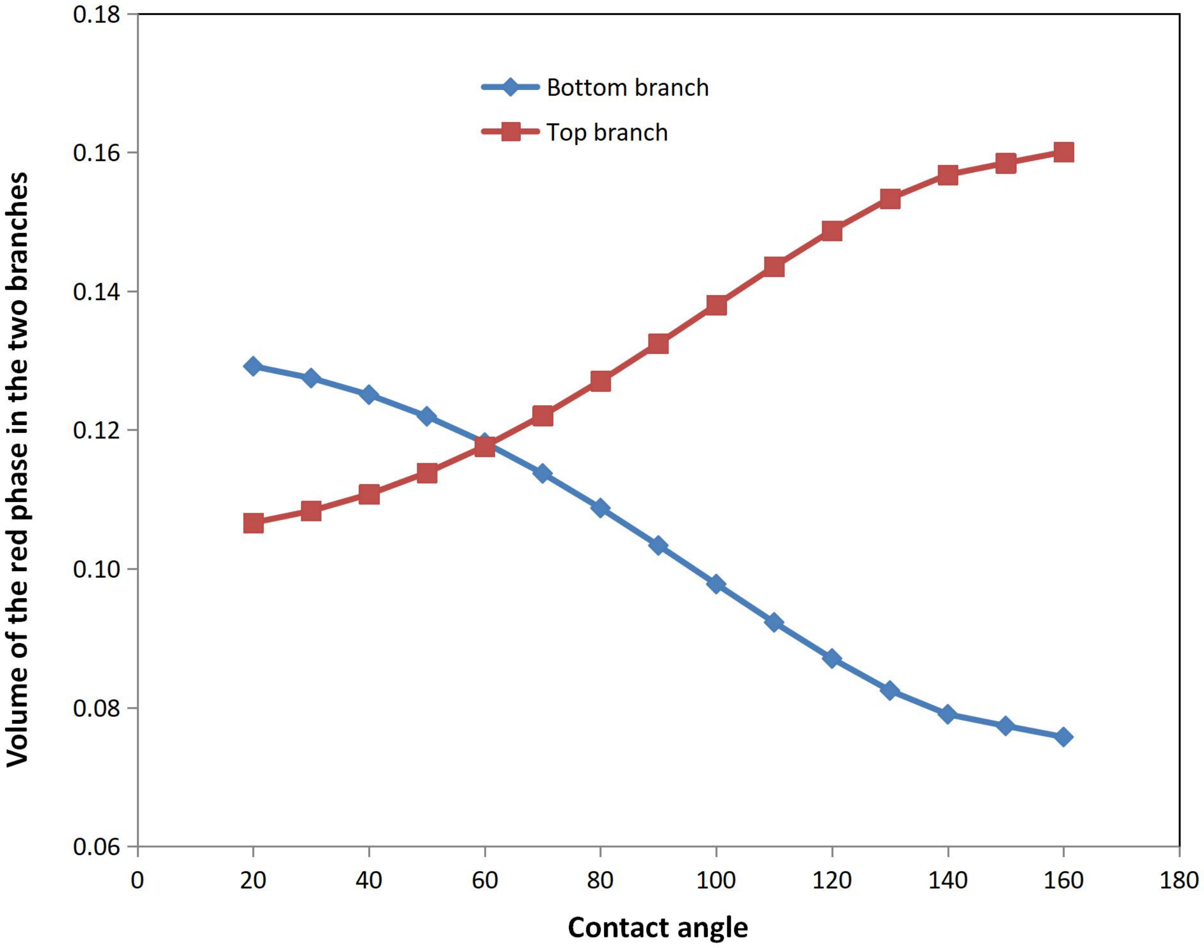

Fig. 10 Volume of the red phase in the two branches for the different contact angle scenarios (EEWWCC)

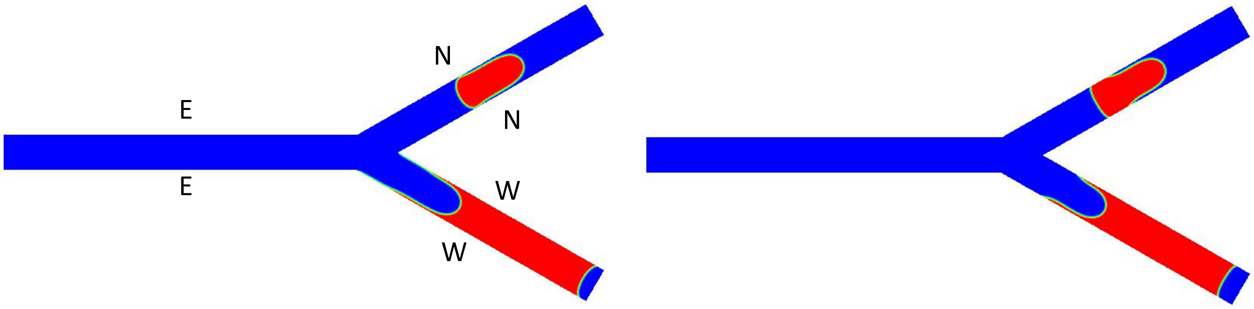

a) Angle 20^{o}

b) Angle 40^{o}

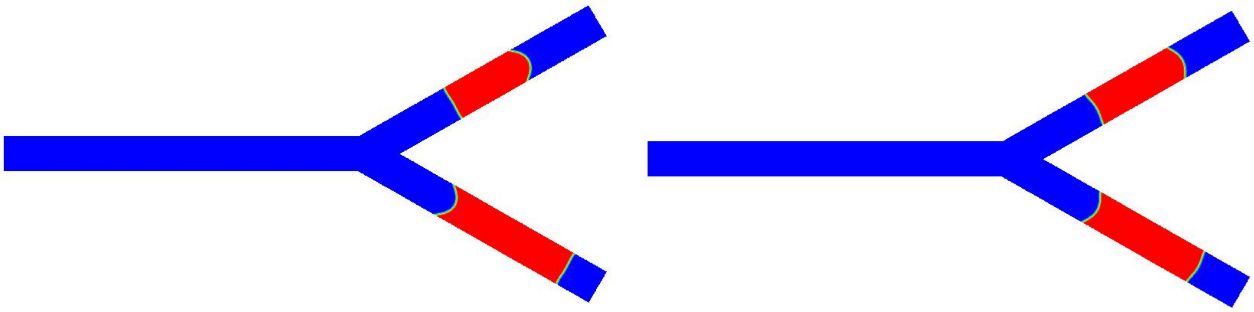

c) Angle 65^{o}

d) Angle 80^{o}

Fig. 11 Different flow configurations of the red phase for different contact angle of the bottom branch for the scenario EENNWW after time= 115 (E: 90^{o}, N+W: 180^{o})

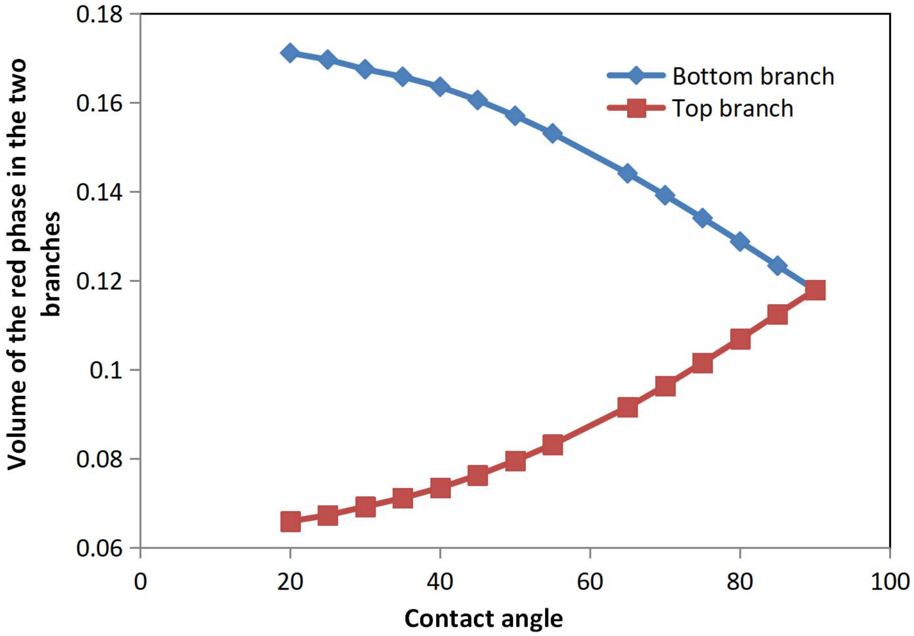

Fig. 12 Volume of the red phase in the two branches for the different contact angle scenarios

(EENNWW)

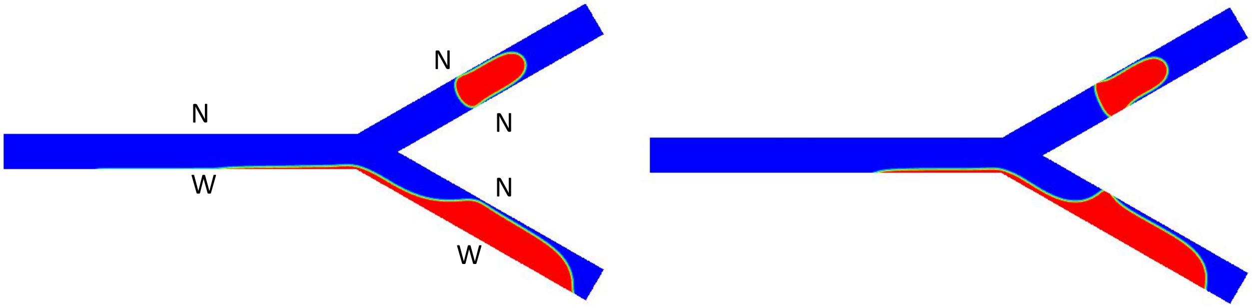

a) Angle 20°

b) Angle 40°

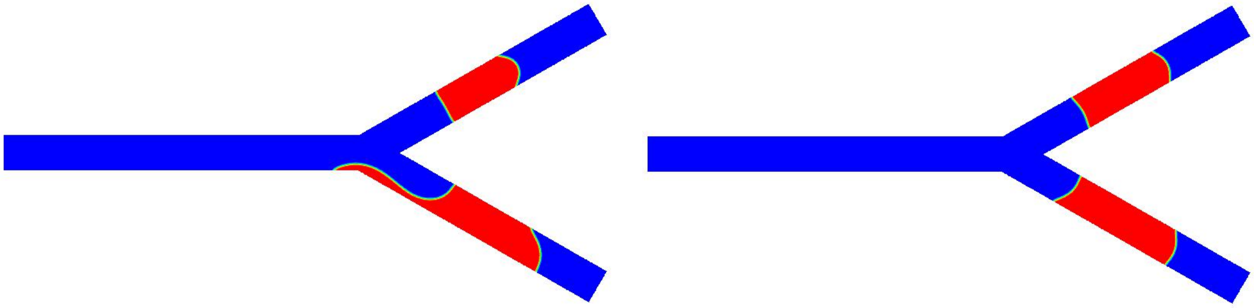

c) Angle 65°

d) Angle 80°

Fig. 13 Different flow configurations of the red phase for different contact angle of the bottom branch for the scenario NWNNNW after time= 105 (N+W: 180°)

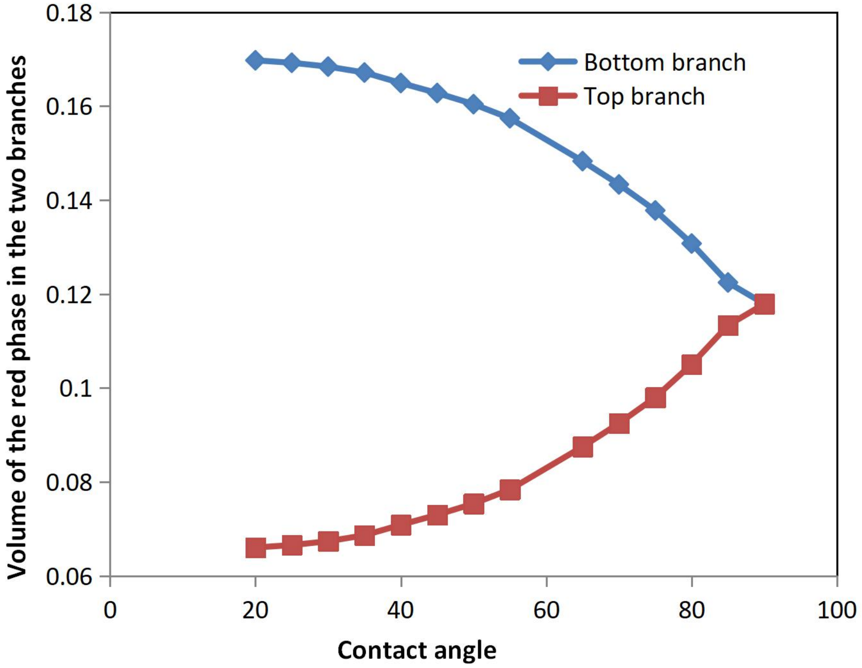

Fig. 14 Volume of the red phase in the two branches for the different contact angle scenarios (NCNNNC)

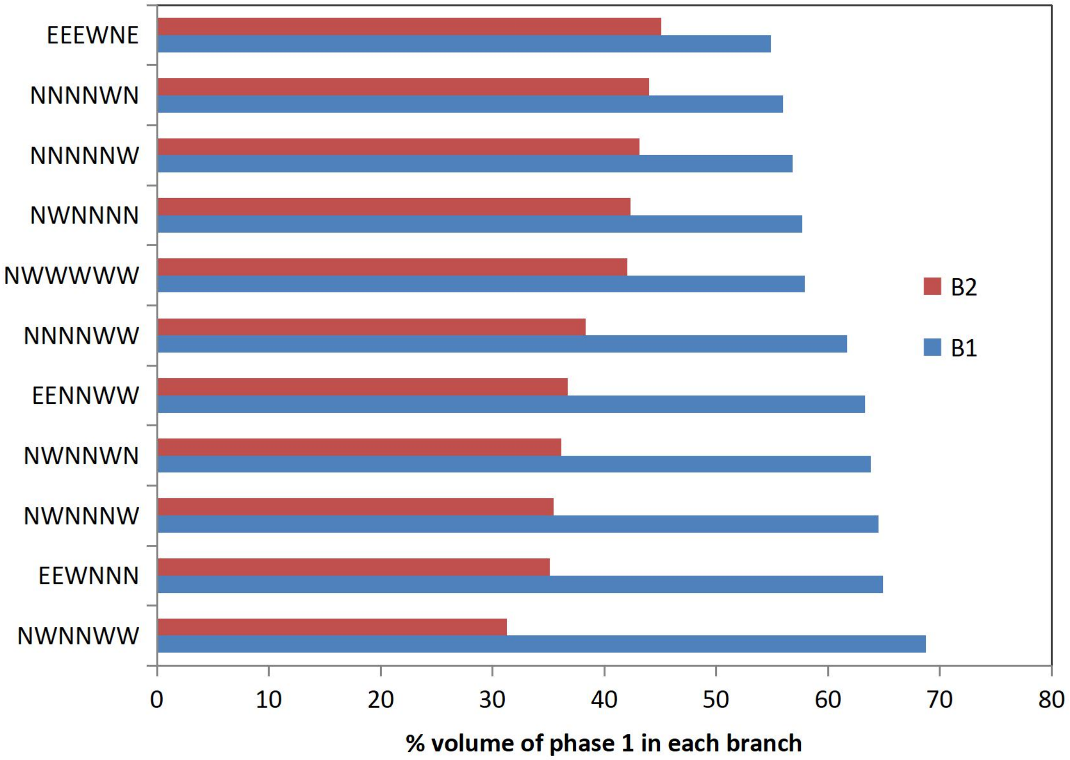

Fig. 15 Comparison of the volume of the red phase in both channels for different wettability scenarios.